Inorganic Chemistry

Article

pubs.acs.org/IC

High-Valent Chromium–Oxo Complex Acting as an Efficient Catalyst Precursor for Selective Two-Electron Reduction of Dioxygen by a Ferrocene Derivative

Shuo Liu,[†,∥] Kentaro Mase,[‡,∥] Curt Bougher,[†] Scott D. Hicks,[†] Mahdi M. Abu-Omar,*[,†] and Shunichi Fukuzumi*[,‡]

[†]Department of Chemistry, Purdue University, 560 Oval Drive, West Lafayette, Indiana 47907, United States

[‡]Department of Material and Life Science, Graduate School of Engineering, Osaka University, ALCA, Japan Science and Technology (JST), Suita, Osaka 565-0871, Japan

Supporting Information

ABSTRACT: Efficient catalytic two-electron reduction of dioxygen (O_2) by octamethylferrocene (Me_8Fc) produced hydrogen peroxide (H_2O_2) using a high-valent chromium(V)–oxo corrole complex, [(tpfc)Cr^{V}(O)] (tpfc = tris(pentafluorophenyl)corrole) as a catalyst precursor in the presence of trifluoroacetic acid (TFA) in acetonitrile (MeCN). The facile two-electron reduction of [(tpfc)Cr^{V}(O)] by 2 equiv of Me_8Fc in the presence of excess TFA produced the corresponding chromium(III) corrole [(tpfc)$Cr^{III}(OH_2)$] via fast electron transfer from Me_8Fc to [(tpfc)Cr^{V}(O)] followed by double protonation of [(tpfc)Cr^{IV}(O)]$^-$ and facile second-electron transfer from Me_8Fc. The rate-determining step in the catalytic two-electron reduction of O_2 by Me_8Fc in the presence of excess TFA is inner-sphere electron transfer from [(tpfc)$Cr^{III}(OH_2)$] to O_2 to produce the chromium(IV) superoxo species [(tpfc)$Cr^{IV}(O_2^{\bullet-})$], followed by fast proton-coupled electron transfer reduction of [(tpfc)$Cr^{IV}(O_2^{\bullet-})$] by Me_8Fc to yield H_2O_2, accompanied by regeneration of [(tpfc)$Cr^{III}(OH_2)$]. Thus, although the catalytic two-electron reduction of O_2 by Me_8Fc was started by [(tpfc)Cr^{V}(O)], no regeneration of [(tpfc)Cr^{V}(O)] was observed in the presence of excess TFA, regardless of the tetragonal chromium complex being to the left of the oxo wall. In the presence of a stoichiometric amount of TFA, however, disproportionation of [(tfpc)Cr^{IV}(O)]$^-$ occurred via the protonated species [(tpfc)Cr^{IV}(OH)] to produce [(tpfc)$Cr^{III}(OH_2)$] and [(tpfc)Cr^{V}(O)].

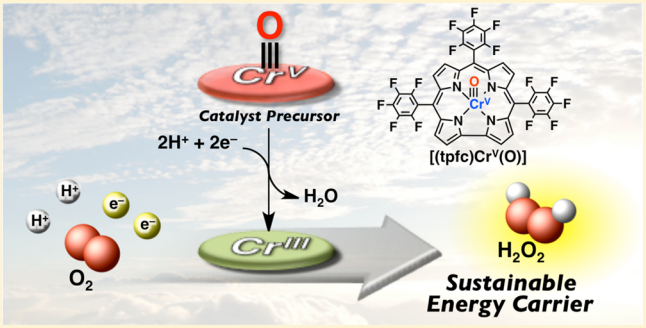

INTRODUCTION

Extensive efforts have been devoted to developing catalysts for four-electron reduction of dioxygen (O_2), because it is of not only great biological interest, such as cytochrome *c* oxidases[1−3] and lacasse,[4−6] but also technological significance such as use in fuel cells.[7,8] Two-electron reduction of O_2 to produce hydrogen peroxide has also merited increasing attention, because hydrogen peroxide is a versatile and environmentally benign oxidizing reagent produced on a large industrial scale. It is also a promising candidate as a sustainable energy carrier with a high energy density that can be used in hydrogen peroxide fuel cells.[9−11] However, the anthraquinone process, currently used to produce hydrogen peroxide industrially, requires potentially explosive hydrogen and a noble metal catalyst. Alternatively, electrocatalysis of metal complexes of iron, cobalt, and copper has been extensively investigated in heterogeneous systems.[7,8,12,13] In contrast to investigations of heterogeneous systems, investigations of the catalytic reduction of O_2 by metal complexes in homogeneous systems have provided valuable mechanistic insight into the role of reaction intermediates in the catalytic cycle.[14−31]

Whereas various metal complexes catalyze the catalytic four-electron reduction of O_2, only late transition-metal complexes have been reported to act as catalysts for selective two-electron reduction of O_2.[29−31] This can be explained by the "oxo wall" theory established by Gray and Winkler in which mononuclear complexes composed of transition metals to the right of the Fe–Ru–Os group in the periodic table with tetragonal geometry will not form a terminal oxo complex due to electrostatic repulsion of electrons between the d orbitals of these metals and the oxo ligand, where electrons in the d orbitals of these metals begin to occupy antibonding orbitals of the M=O unit.[32,33] Thus, metal complexes composed of metals to the right of the Fe–Ru–Os group catalyze selective two-electron reduction of O_2 to produce H_2O_2 via M–O bond cleavage of hydroperoxo intermediate, as shown in Scheme 1a.[29−31]

In contrast, even mononuclear complexes composed of metals to the right of the Fe–Ru–Os group can catalyze the

Received: June 10, 2014
Published: July 2, 2014

dx.doi.org/10.1021/ic5013457 | Inorg. Chem. 2014, 53, 7780–7788

Scheme 1

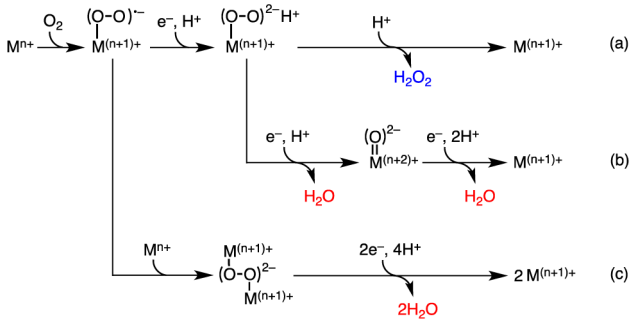

four-electron reduction of O_2 via the formation of dinuclear peroxo complexes, which act as key intermediates followed by homolytic O−O bond cleavage to produce H_2O (Scheme 1c).[24−28] Except for the dinuclear copper complex reported by Karlin and co-workers,[31] it is well-known that Cu^I reacts with O_2 to afford the superoxo species, which reacts rapidly with a second equivalent of Cu^I to form dinuclear peroxo species, followed by further reduction in the presence of acid to facilitate the four-electron reduction of O_2 to produce H_2O.[24]

Consequently, metal complexes composed of early transition metals to the left of Fe−Ru−Os group are thought to catalyze selective four-electron reduction of O_2 via the formation of stable metal oxo complexes, as shown in Scheme 1b. However, there has been no report on the catalytic reduction of O_2 and its selectivity using chromium complexes.

Contrary to what we expected from the reaction shown in Scheme 1b, we have found that selective two-electron reduction of O_2 by ferrocene derivatives as a one-electron reductant is catalyzed by chromium(V)−oxo tris(pentafluorophenyl)corrole ([(tpfc)Cr^V(O)]) in the presence of trifluoroacetic acid (TFA) in acetonitrile (MeCN) at 298 K under homogeneous conditions. We report herein the mechanism of the catalytic O_2 reduction and its selectivity by octamethylferrocene (Me_8Fc) with [(tpfc)Cr^V(O)] in the presence of TFA, on the basis of detailed kinetic studies of each step in the catalytic cycle and the overall catalytic reaction and detection of reactive intermediates.

EXPERIMENTAL SECTION

General Procedure. Chemicals were purchased from commercial sources and used without further purification, unless otherwise noted. Acetonitrile (MeCN) used for spectroscopic and electrochemical measurements was dried with calcium hydride and distilled under nitrogen (N_2) prior to use.[34] Chromium(V)−oxo tris(pentafluorophenyl)corrole [(tpfc)Cr^V(O)] has been synthesized and characterized as reported previously.[35,36] Octamethylferrocene (Me_8Fc) was purchased commercially and purified by sublimation. Tetra-*n*-butylammonium hexafluorophosphate ($TBAPF_6$) was twice recrystallized from ethanol and dried in vacuo prior to use. MALDI−TOF MS measurements were performed on a Kratos Compact MALDI I mass spectrometer (Shimadzu) for the detection of [(tpfc)Cr^{IV}]$^+$, using dithranol as a matrix in the reflectron-positive mode.

Spectroscopic and Kinetic Measurements. UV−vis spectroscopy was carried out on a Hewlett-Packard 8453 diode array spectrophotometer at room temperature using 1.00 cm cells. Rate constants of oxidation of Me_8Fc by O_2 in the presence of a catalytic amount of [(tpfc)Cr^V(O)] and an excess amount of TFA in MeCN at 298 K were determined by monitoring the appearance of absorption bands due to the corresponding ferrocenium ions (Fc^+, λ_{max} = 620 nm, ε_{max} = 330 M^{-1} cm^{-1}; Me_8Fc^+, λ_{max} = 750 nm, ε_{max} = 410 M^{-1} cm^{-1}).[30] At the monitored wavelengths, spectral overlap was observed with [(tpfc)Cr^{IV}(O)]$^-$ (λ = 620 nm (ε = 5.4 × 10^3 M^{-1} cm^{-1}), λ = 750 nm (ε = 3.6 × 10^3 M^{-1} cm^{-1})). Typically, the concentration of Me_8Fc employed for the catalytic reduction of O_2 was much larger than that of O_2, when O_2 is the reaction-limiting reagent in the reaction solution. In contrast, the small amount of Me_8Fc used for the reduction of O_2 was employed in an O_2-saturated MeCN solution, when Me_8Fc is the reaction-limiting reagent. The limiting concentration of O_2 in a MeCN solution was prepared by a mixed gas flow of O_2 and N_2. The mixed gas was controlled by using a gas mixer (Kofloc GB-3C, KOJIMA Instruments, Inc.) that can mix two or more gases at a certain pressure and flow rate. The concentration of O_2 in an air-saturated MeCN solution (2.6 × 10^{-3} M) was determined as reported previously.[37]

The amount of hydrogen peroxide (H_2O_2) formed was determined by titration with iodide ion: A diluted CH_3CN solution (2.0 mL) of the product mixture (250 μL) was treated with an excess amount of NaI, and the amount of I_3^- formed was determined by the absorption spectrum (λ_{max} = 361 nm, ε = 2.8 × 10^4 M^{-1} cm^{-1}).[38]

Kinetic measurements for fast reactions with short half-lifetimes (within 10 s) were performed on a UNISOKU RSP-601 stopped-flow spectrophotometer with an MOS-type high selective photodiode array at 298 K using a Unisoku thermostated cell holder. Rates of electron transfer from Me_8Fc to [(tpfc)Cr^{IV}(O)]$^-$ were monitored by the decay of absorption bands due to [(tpfc)Cr^{IV}(O)]$^-$.

Electrochemical Measurements. Cyclic voltammetry (CV) measurements were performed on an ALS 630B electrochemical analyzer, and voltammograms were measured in deaerated MeCN containing 0.10 M $TBAPF_6$ as a supporting electrolyte at room temperature. A conventional three-electrode cell was used with a glassy carbon working electrode (surface area of 2.8 × 10 mm^2) or a platinum working electrode (surface area of 8.0 mm^2) and a platinum wire as the counter electrode. The glassy carbon working electrode (BAS) and the platinum working electrode (BAS) were routinely polished with BAS polishing alumina suspension and rinsed with acetone before use. The potentials were measured with respect to the Ag/$AgNO_3$ (1.0 × 10^{-2} M) reference electrode. All potentials (vs Ag/$AgNO_3$) were converted to values vs SCE by adding 0.29 V.[39] Redox potentials were determined using the relation $E_{1/2}$ = (E_{pa} + E_{pc})/2.

Electron Paramagnetic Resonance (EPR) Measurements. The EPR spectra were performed on a JEOL X-band EPR spectrometer (JES-ME-LX) using a quartz EPR tube containing a deaerated sample frozen solution at 80 K. The internal diameter of the EPR tube is 4.0 mm, which is small enough to fill the EPR cavity but large enough to obtain good signal-to-noise ratios during the EPR measurements at low temperatures (80 K). The EPR spectra were measured under nonsaturating microwave power conditions. The amplitude of modulation was chosen to optimize the resolution and the signal-to-noise (S/N) ratio of the observed spectra. The *g* values were calibrated with a Mn^{2+} marker.

RESULTS AND DISCUSSION

Electron Transfer from Me_8Fc to [(tpfc)Cr^V(O)]. When octamethylferrocene (Me_8Fc) was employed as a one-electron reductant, electron transfer from Me_8Fc to [(tpfc)Cr^V(O)] occurred rapidly, generating octamethylferrocenium ion (Me_8Fc^+) and [(tpfc)Cr^{IV}(O)]$^-$, as given by eq 1.

$$Me_8Fc + [(tpfc)Cr^V(O)] \rightarrow Me_8Fc^+ + [(tpfc)Cr^{IV}(O)]^- \quad (1)$$

The absorption bands at 400 (analogue to the Soret band in porphyrins) and 556 nm (analogue to the Q-band in porphyrins) associated with [(tpfc)Cr^V(O)] decreased smoothly, accompanied by an increase in the absorption bands at 430 and 577 nm with clean isosbestic points (Figure 1a). The latter bands are assigned to [(tpfc)Cr^{IV}(O)]$^-$, as reported previously.[35,36] The stoichiometry of the electron-transfer reaction (eq 1) was confirmed by the spectral titration

dx.doi.org/10.1021/ic5013457 | Inorg. Chem. 2014, 53, 7780−7788

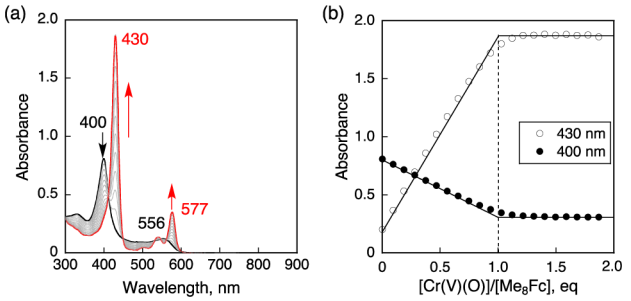

Figure 1. (a) Absorption spectral changes of $[(tpfc)Cr^{V}(O)]$ (1.0×10^{-5} M) upon the addition of Me_8Fc in air-saturated MeCN at 298 K. (b) Absorbance changes at 400 (closed circle) and 430 nm (open circle) upon the addition of Me_8Fc.

at 400 and 430 nm, and no further reduction of $[(tpfc)Cr^{IV}(O)]^{-}$ occurred, as shown in Figure 1b.

Reduction of $[(tpfc)Cr^{IV}(O)]^{-}$ by Me_8Fc. In the presence of a stoichiometric amount of TFA (proton source), further spectral changes occurred to produce 0.5 equiv of $[(tpfc)Cr^{V}(O)]$ and $[(tpfc)Cr^{III}(OH_2)]$, where the absorption bands at 400 and 648 nm appeared due to $[(tpfc)Cr^{V}(O)]$ and $[(tpfc)Cr^{III}(OH_2)]$[35,36], respectively, accompanied by a decrease in the absorption bands at 430 and 577 nm due to $[(tpfc)Cr^{IV}(O)]^{-}$, as shown in Figure 2. The decay rate of

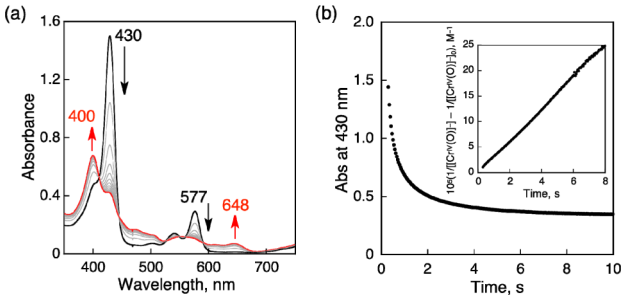

Figure 2. Absorption spectral changes of $[(tpfc)Cr^{IV}(O)]^{-}$ (1.0×10^{-5} M) upon the addition of TFA (1.0×10^{-5} M) in deaerated MeCN at 298 K. (b) Time profile of the absorbance at 430 nm upon the addition of TFA. Inset shows second-order plot.

$[(tpfc)Cr^{IV}(O)]^{-}$ obeys second-order kinetics, as shown in a linear second-order plot (inset of Figure 2b). Such second-order kinetics, together with the appearances of $[(tpfc)Cr^{V}(O)]$ and $[(tpfc)Cr^{III}(OH_2)]$ associated with the decay of $[(tpfc)Cr^{IV}(O)]^{-}$, can be well explained by the disproportionation of $[(tpfc)Cr^{IV}(O)]^{-}$, which is protonated in the presence of TFA (i.e., $[(tpfc)Cr^{IV}(OH)]$) to afford 0.5 equiv of $[(tpfc)Cr^{V}(O)]$ and $[(tpfc)Cr^{III}(OH_2)]$, as given by eq 2. The kinetic equation is given by eq 3. The rate constant of the disproportionation of $[(tfpc)Cr^{IV}(O)^{-}]$ (k_{dispro}) was determined to be 3.1×10^{5} M^{-1} s^{-1} on the basis of the second-order plot (inset of Figure 2b).

$$2[(tpfc)Cr^{IV}(O)] + 2H^{+} \rightarrow [(tpfc)Cr^{V}(O)] + [(tpfc)Cr^{III}(OH_2)] \quad (2)$$

$$-d[(tpfc)Cr^{IV}(O)^{-}]/dt = k_{dispro}[(tpfc)Cr^{IV}(O)^{-}]^{2} \quad (3)$$

Upon the addition of an excess amount of TFA to the solution of $[(tpfc)Cr^{IV}(O)]^{-}$ containing Me_8Fc in deaerated MeCN at 298 K, the rise of the absorption band at 648 nm due to $[(tpfc)Cr^{III}(OH_2)]$ accompanied by the decay of the absorption bands at 430 and 577 nm due to $[(tpfc)Cr^{IV}(O)]^{-}$ was observed using stopped-flow technique (Figure 3). In the

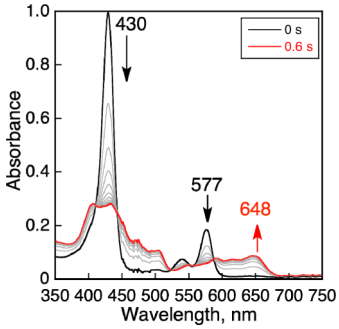

Figure 3. Absorption spectral changes of $[(tpfc)Cr^{IV}(O)]^{-}$ (5.5×10^{-6} M) upon the addition of TFA (7.5×10^{-5} M) in the presence of Me_8Fc (1.0×10^{-4} M) in deaerated MeCN at 298 K. The black and red lines show the spectra before and after the addition of TFA, respectively.

presence of excess TFA and Me_8Fc, the decay of $[(tpfc)Cr^{IV}(O)]^{-}$ obeyed first-order kinetics, as shown in Figure 4a.

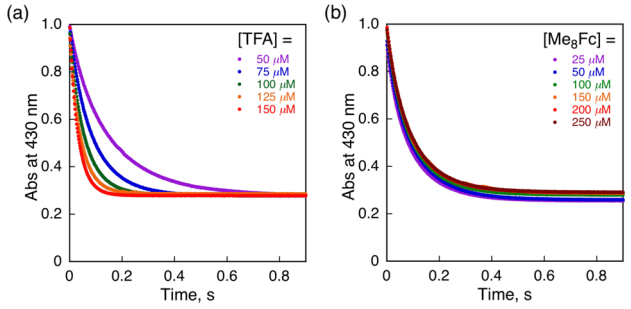

Figure 4. Time profiles of absorbance at 430 nm due to the decrease of $[(tpfc)Cr^{IV}(O)]^{-}$ in the reduction of $[(tpfc)Cr^{IV}(O)]^{-}$ (5.5×10^{-6} M) (a) by Me_8Fc (1.0×10^{-4} M) in the presence of various concentrations of TFA in deaerated MeCN at 298 K and (b) by various concentrations of Me_8Fc in the presence of TFA (7.5×10^{-5} M) in deaerated MeCN at 298 K.

The observed rate constants k_{obs} increased with increasing TFA concentration, exhibiting second-order dependence on [TFA] at lower concentration of TFA and first-order dependence on [TFA] at higher concentration of TFA (Figure 5a). Addition-

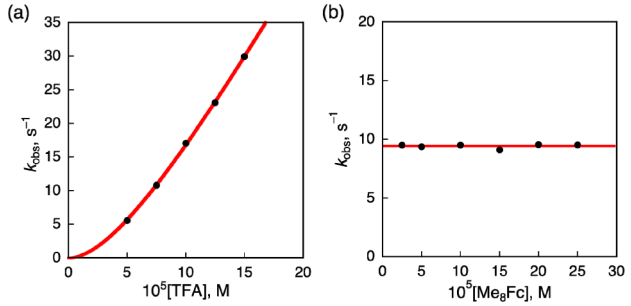

Figure 5. (a) Plot of k_{obs} vs [TFA] for the reduction of $[(tpfc)Cr^{IV}(O)]^{-}$ (5.5×10^{-6} M) by Me_8Fc (1.0×10^{-4} M) in the presence of various concentrations of TFA in deaerated MeCN at 298 K. (b) Plot of k_{obs} vs $[Me_8Fc]$ for the reduction of $[(tpfc)Cr^{IV}(O)]^{-}$ (5.5×10^{-6} M) by various concentrations of Me_8Fc in the presence of TFA (7.5×10^{-5} M) in deaerated MeCN at 298 K.

dx.doi.org/10.1021/ic5013457 | Inorg. Chem. 2014, 53, 7780−7788

ally, the zero-order dependence of k_{obs} on the concentration of Me_8Fc (Figure 5b) indicates that the reduction of $[(tpfc)Cr^{IV}(O)]^-$ occurs via the proton transfer from TFA to $[(tpfc)Cr^{IV}(O)]^-$ to form $[(tpfc)Cr^{IV}(OH)]$ as an intermediate in a pre-equilibrium step, followed by the rate-determining second protonation of $[(tpfc)Cr^{IV}(OH)]$ to afford $[(tpfc)Cr^{IV}(OH_2)]^+$, which is reduced by fast electron transfer from Me_8Fc to $[(tpfc)Cr^{IV}(OH_2)]^+$ to produce $[(tpfc)Cr^{III}(OH_2)]$, as shown in Scheme 2.

Scheme 2

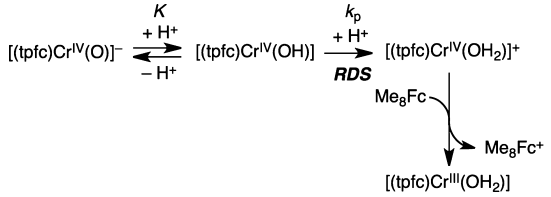

According to Scheme 2, the decay rate of $[(tpfc)Cr^{IV}(O)]^-$ is given by eq 4,

$$-d[(tpfc)Cr^{IV}(O)^-]_t/dt = k_p[(tpfc)Cr^{IV}(OH)][H^+] \quad (4)$$

where $[(tpfc)Cr^{IV}(O)^-]_t$ is the total concentration of $[(tpfc)Cr^{IV}(O)]^-$ and $[(tpfc)Cr^{IV}(OH)]$. The concentration of $[(tpfc)Cr^{IV}(OH)]$ is given by eq 5.

$$[(tpfc)Cr^{IV}(OH)] = K[(tpfc)Cr^{IV}(O)]_t[H^+]/(1 + K[H^+]) \quad (5)$$

Thus, by combining eqs 4 and 5, we obtain eq 6, which agrees with the observed dependence of k_{obs} on $[H^+]$.

$$-d[(tpfc)Cr^{IV}(O)^-]_t/dt = k_pK[(tpfc)Cr^{IV}(O)^-]_t[H^+]^2/(1 + K[H^+]) \quad (6)$$

Electrochemical Measurements. Electrochemical measurements of $[(tpfc)Cr^{V}(O)]$ were performed in deaerated MeCN containing 0.10 M $TBAPF_6$ to determine the catalytic activity of $[(tpfc)Cr^{V}(O)]$ toward the reduction of O_2, as shown in Figure 6. In the absence of TFA, reversible redox couples of $[(tpfc)Cr^{V}(O)]/[(tpfc)Cr^{IV}(O)]^-$ and $[(tpfc^{\bullet+})Cr^{V}(O)]^+/[(tpfc)Cr^{V}(O)]$ were observed at $E_{1/2}$ versus SCE values of 0.13 and 1.14 V, respectively,[35,36] as shown in Figure 6a (black). In the presence of TFA, the redox wave for $[(tpfc^{\bullet+})Cr^{V}(O)]^+/[(tpfc)Cr^{V}(O)]$ was unchanged at 1.14 V, whereas the redox potential for $[(tpfc)Cr^{V}(O)]/[(tpfc)Cr^{IV}(O)]^-$ was shifted to a more positive potential (Figure 6a, red). A single irreversible reduction at E_{pc} = 0.17 V coupled with an irreversible oxidation peak at E_{pa} = 0.45 V is observed at a scan rate of 0.1 V s^{-1}, where the oxidation peak is assigned to the oxidation of $[(tpfc)Cr^{III}(OH_2)]$ produced by the disproportionation of $[(tpfc)Cr^{IV}(OH)]$ formed in the course of the reduction of $[(tpfc)Cr^{V}(O)]$ in the presence of TFA. The redox wave for $[(tpfc)Cr^{IV}]^+/[(tpfc)Cr^{III}(OH_2)]$ was confirmed by examining a deaerated MeCN solution of $[(tpfc)Cr^{III}(OH_2)]$ prepared independently by adding 2 equiv of Me_8Fc (2.0×10^{-3} M) in the presence of TFA (Figure S3, Supporting Information). The reversible redox couple for $[(tpfc)Cr^{IV}]^+/[(tpfc)Cr^{III}(OH_2)]$ was observed at $E_{1/2}$ = 0.37 V, where the oxidation peak of $[(tpfc)Cr^{III}(OH_2)]$ (E_{pa} = 0.45 V) is virtually the same as that observed in Figure 6a. Thus, the

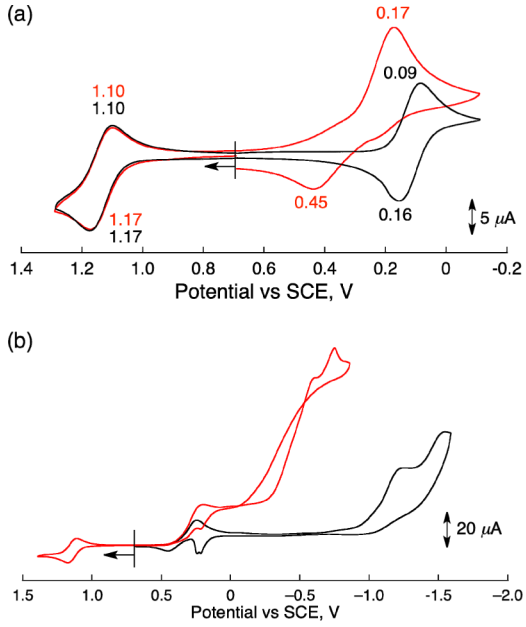

Figure 6. Cyclic voltammograms of (a) a N_2-saturated MeCN solution of $[(tpfc)Cr^{V}(O)]$ (1.0×10^{-3} M) recorded in the presence of 0.10 M $TBAPF_6$ without TFA (black line), with TFA (1.0×10^{-2} M) (red line) and a sweep rate of 0.1 V s^{-1}, and (b) $[(tpfc)Cr^{V}(O)]$ (1.0×10^{-3} M) recorded in the presence of 0.10 M $TBAPF_6$ with TFA (1.0×10^{-2} M) in a N_2-saturated MeCN solution (black line), in an O_2-saturated MeCN solution (red line) and a sweep rate of 0.02 V s^{-1}.

electron-transfer reduction of $[(tpfc)Cr^{V}(O)]$ is followed by disproportionation of $[(tpfc)Cr^{IV}(OH)]$ in the presence of TFA.

The catalytic current was observed in the presence of $[(tpfc)Cr^{V}(O)]$, as shown in Figure 6b, where the catalytic current at −0.25 V is much larger than the current without $[(tpfc)Cr^{V}(O)]$, as shown in Figure S4 (Supporting Information). Hydrogen production processes have been observed with onset potential of around −0.5 V (vs SCE) in a N_2-saturated MeCN solution, as shown in Figure S5 (Supporting Information), which is significantly more negative that the onset potential for the catalytic O_2 reduction in Figure 6b.

Catalytic Two-Electron Reduction of O_2 by Me_8Fc with $[(tpfc)Cr^{V}(O)]$ in the Presence of TFA. The addition of TFA to a MeCN solution containing a catalytic amount of $[(tpfc)Cr^{V}(O)]$, excess Me_8Fc, and O_2 at 298 K results in the efficient oxidation of Me_8Fc by O_2 to afford Me_8Fc^+ (Figure 7). It should be noted that the oxidation of Me_8Fc by O_2 hardly occurred in the absence of $[(tpfc)Cr^{V}(O)]$ under the present experimental conditions (Figure S6, Supporting Information). The stoichiometry of the catalytic oxygen reduction was confirmed under the employed reaction conditions with limited concentration of O_2 relative to the concentration of Me_8Fc and TFA (i.e., $[O_2] \ll [Me_8Fc], [TFA]$). The formation of Me_8Fc^+ was monitored by a rise in absorbance at 750 nm, as shown in Figure 7a. Figure 7b shows the time course of formation of Me_8Fc^+ in the reduction of limited concentration of O_2 (3.3×10^{-4} M). At the end of the catalytic reaction, the concentration of Me_8Fc^+ (6.6×10^{-4} M) formed in the catalytic reduction of O_2 by Me_8Fc is twice of the concentration of O_2 (3.3×10^{-4} M) in MeCN. This result clearly indicates that the two-electron reduction of O_2 occurs to produce 2 equiv of Me_8Fc^+, and there is no further reduction to produce more than 2 equiv of Me_8Fc^+, as given by eq 7.

dx.doi.org/10.1021/ic5013457 | Inorg. Chem. 2014, 53, 7780−7788

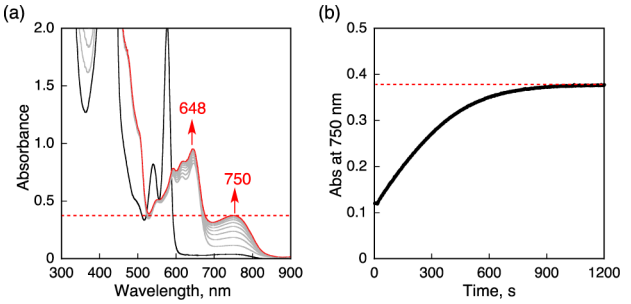

Figure 7. (a) Absorption spectral changes in the two-electron reduction of O_2 (3.3×10^{-4} M) by Me_8Fc (8.0×10^{-3} M) with $[(tpfc)Cr^{V}(O)]$ (5.0×10^{-5} M) in the presence of TFA (2.5×10^{-2} M) in MeCN at 298 K. The black and red lines show the spectra before and after injection of O_2, respectively. The dotted line is the absorbance at 750 nm due to 6.6×10^{-4} M of Me_8Fc^+. (b) Time profile of absorbance at 750 nm due to the formation of Me_8Fc^+.

$$O_2 + 2H^+ + 2Me_8Fc \xrightarrow[Cat]{} H_2O_2 + 2Me_8Fc^+ \quad (7)$$

The stoichiometry of the catalytic reduction of O_2 by Me_8Fc with $[(tpfc)Cr^{V}(O)]$ was further confirmed by changing O_2 concentration (Figure S7, Supporting Information). In each concentration of O_2, the concentration of Me_8Fc^+ formed in the catalytic reduction of O_2 by Me_8Fc is twice the concentration of O_2.

In addition, the formation of the stoichiometric amount of H_2O_2 was confirmed by the iodometric titration experiments (Figure S8, Supporting Information).[38] This means that the chromium corrole complex is quite stable, even in the presence of acidic solution by the strong electrostatic interaction between the multiply charged chromium ion and the corrole ligand. The time profile of the formation of Me_8Fc^+ obeyed first-order kinetics under the conditions of $[O_2] \ll [Me_8Fc]$ (Figure 7b). This suggests that the catalytic rate is first order with respect to O_2 concentration. During the catalytic reaction, $[(tpfc)Cr^{V}(O)]$ is converted to $[(tpfc)Cr^{III}(OH_2)]$, as shown by the gray line spectrum with λ_{max} = 648 nm in Figure 7a, which agrees with the absorption spectrum of $[(tpfc)Cr^{III}(OH_2)]$ produced by the reduction of $[(tpfc)Cr^{V}(O)]$ in the presence of TFA in deaerated MeCN in Figure 3. These results suggest that the oxidation of $[(tpfc)Cr^{III}(OH_2)]$ by O_2 is the rate-determining step in the catalytic reaction. The turnover number was determined to be more than 480, as shown in Figure S9 (Supporting Information).

Under reaction conditions such that $[Me_8Fc] \ll [O_2]$, [TFA], the time profiles of the formation of Me_8Fc^+ obeyed zero-order kinetics (Figure 8b), because the large excess O_2 concentration remains nearly constant when the rate also remains constant, irrespective of a decrease in the concentration of Me_8Fc. When the catalytic reaction was over, a sharp spectral change in absorbance at 648 nm due to $[(tpfc)Cr^{III}(OH_2)]$ was observed at around 22 s (Figure 8b). This spectral change at the end of the catalytic reaction is ascribed to the formation of $[(tpfc)Cr^{IV}]^+$, formed by the oxidation of $[(tpfc)Cr^{III}(OH_2)]$ with O_2 once all Me_8Fc was consumed. The formation of $[(tpfc)Cr^{IV}]^+$ observed at the end of the catalytic reaction was confirmed by comparison with the absorption spectrum of $[(tpfc)Cr^{IV}]^+$, which was produced independently by the addition of 2 equiv of Me_8Fc (5.0×10^{-5} M) to an air-saturated MeCN solution of $[(tpfc)Cr^{V}(O)]$ (2.5×10^{-5} M) in the presence of a large excess amount of TFA, as shown in

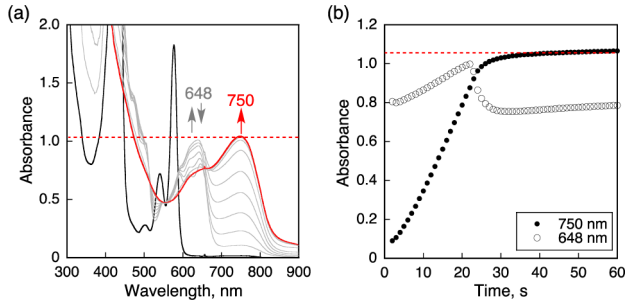

Figure 8. (a) Absorption spectral changes in the two-electron reduction of O_2 (1.3×10^{-2} M) by Me_8Fc (2.0×10^{-3} M) with $[(tpfc)Cr^{V}(O)]$ (5.0×10^{-5} M) in the presence of TFA (2.5×10^{-2} M) in O_2-saturated MeCN at 298 K. The black and red lines show the spectra before and after the addition of TFA, respectively. The dotted line is the absorbance at 750 nm due to 2.0×10^{-3} M of Me_8Fc^+. (b) Time profile of absorbance at 750 nm due to the formation of Me_8Fc^+.

Figure 9a. This reaction intermediate is further supported by the appearance on the MALDI TOF mass spectrum of an ionic

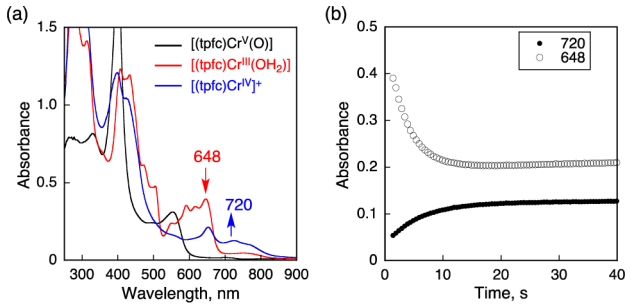

Figure 9. Absorption spectral changes of $[(tpfc)Cr^{V}(O)]$ (2.5×10^{-5} M) upon the addition of Me_8Fc (5.0×10^{-5} M) in the presence of TFA (1.0×10^{-2} M) in air-saturated MeCN at 298 K. The black line shows the spectrum before the addition of Me_8Fc. The red line shows the spectrum just after the addition of Me_8Fc, which represents $[(tpfc)Cr^{III}(OH_2)]$. The blue line shows the spectrum observed at around 40 s after the addition of Me_8Fc, which represents a putative $[(tpfc)Cr^{IV}]^+$. (b) Absorbance changes at 648 nm (○) and 720 nm (●) upon the addition of Me_8Fc.

pattern at 845.58, which is attributed to chromium corrole species without an oxo ligand (Figure S10, Supporting Information). The time course is shown in Figure 9b, where $[(tpfc)Cr^{V}(O)]$ was rapidly reduced by 2 equiv of Me_8Fc to produce $[(tpfc)Cr^{III}(OH_2)]$ (λ = 648nnm), which was subsequently oxidized by O_2 to produce $[(tpfc)Cr^{IV}]^+$ (λ = 720 nm).

Kinetics and Mechanism of Two-Electron Reduction of O_2 by Me_8Fc with $[(tpfc)Cr^{V}(O)]$. The kinetics of the catalytic two-electron reduction of O_2 by Me_8Fc with $[(tpfc)Cr^{V}(O)]$ was investigated by following an increase in absorbance at 750 nm due to Me_8Fc^+ under Me_8Fc limiting conditions (Figure S11, Supporting Information). The pseudo-zero-order rate constant (k_{obs}) is proportional to the concentration of $[(tpfc)Cr^{V}(O)]$ and that of O_2 (Figure 10a,d), whereas the k_{obs} values remained constant, irrespective of the change in concentrations of Me_8Fc and that of TFA (Figure 10b,c). The first-order dependences on the concentrations of $[(tpfc)Cr^{V}(O)]$ and O_2 indicate that inner-sphere electron transfer from $[(tpfc)Cr^{III}(OH_2)]$ to O_2 to give

dx.doi.org/10.1021/ic5013457 | Inorg. Chem. 2014, 53, 7780−7788

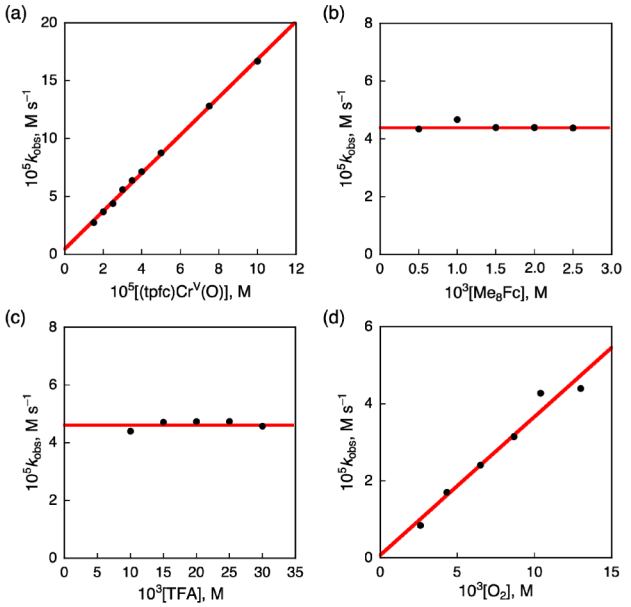

Figure 10. Plot of (a) k_{obs} vs [(tpfc)Cr^V(O)] for the two-electron reduction of O_2 (1.3×10^{-2} M) by Me_8Fc (1.5×10^{-3} M) in the presence of TFA (1.0×10^{-2} M) in O_2-saturated MeCN. (b) Plot of k_{obs} vs [Me_8Fc] for the two-electron reduction of O_2 (1.3×10^{-2} M) by various concentrations of Me_8Fc with [(tpfc)Cr^V(O)] (2.5×10^{-5} M) in the presence of TFA (1.0×10^{-2} M) in MeCN at 298 K. (c) Plot of k_{obs} vs [Me_8Fc] for the two-electron reduction of O_2 (1.3×10^{-2} M) by Me_8Fc (1.5×10^{-3} M) with [(tpfc)Cr^V(O)] (2.5×10^{-5} M) in the presence of various concentrations of TFA in MeCN at 298 K. (d) Plot of k_{obs} vs [O_2] for the two-electron reduction of various concentrations of O_2 by Me_8Fc (1.5×10^{-3} M) with [(tpfc)Cr^V(O)] (2.5×10^{-5} M) in the presence of TFA (1.0×10^{-2} M) in MeCN at 298 K.

[(tpfc)Cr^{IV}($O_2^{\bullet-}$)], where the aqua ligand is replaced by $O_2^{\bullet-}$, is the rate-determining step in the catalytic cycle, as shown in Scheme 3. The produced [(tpfc)Cr^{IV}($O_2^{\bullet-}$)] is reduced rapidly

Scheme 3

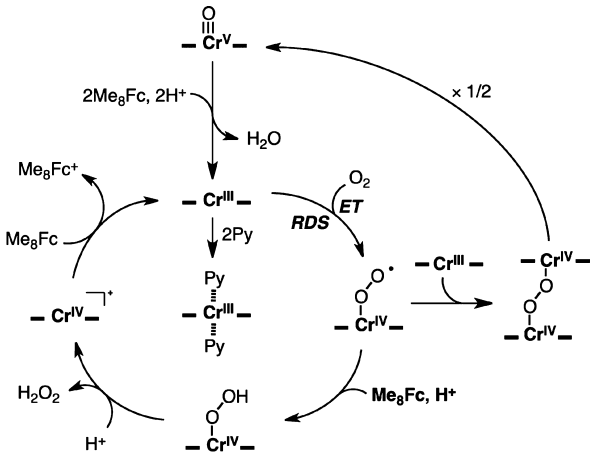

by Me_8Fc with H^+ to produce [(tpfc)Cr^{IV}(OOH)], which is protonated to produce [(tpfc)Cr^{IV}]$^+$ and H_2O_2. The rate-determining electron transfer from [(tpfc)Cr^{III}(OH_2)] to O_2 is also supported by the steady-state appearance of [(tpfc)-Cr^{III}(OH_2)] as the observable intermediate in the catalytic cycle (vide supra). When pyridine (Py) was employed under same experimental conditions as in Figure 10, the catalytic O_2 reduction was inhibited due to the coordination of pyridine to the reaction center of chromium(III) species to form a 6-coordinated state, exhibiting the spectrum of chromium(III) species (Figure S12, Supporting Information), as reported previously.[41]

On the other hand, [(tpfc)Cr^{IV}]$^+$ prepared under single-turnover conditions (Figure 9) is rapidly reduced by Me_8Fc to regenerate [(tpfc)Cr^{III}], where the reaction was too fast to determine the rate constant accurately. This is reasonable, because the one-electron reduction potential of [(tpfc)Cr^{IV}]$^+$ (E_{red} vs SCE = 0.37 V in Figure S1, Supporting Information) is much more positive than the one-electron oxidation potential of Me_8Fc (E_{ox} = −0.04 V vs SCE),[30] when electron transfer from Me_8Fc to [(tpfc)Cr^{IV}]$^+$ is highly exergonic with the driving force of 0.41 eV. When Me_8Fc was replaced by ferrocene (Fc: E_{ox} vs SCE = 0.37 V)[30] as a weaker reductant than Me_8Fc, the catalytic two-electron reduction of O_2 by Fc also occurred as shown in Figure S13, Supporting Information. However, the rate of formation of Fc^+ became much slower than that of Me_8Fc^+, where the absorption band due to [(tpfc)Cr^{IV}]$^+$ was observed during the catalytic reaction. This indicates that the rate-determining step is changed from the oxidation of [(tpfc)Cr^{III}(OH_2)] by O_2 to the reduction of [(tpfc)Cr^{IV}]$^+$ by Fc, because the driving force of electron transfer from Fc to [(tpfc)Cr^{IV}]$^+$ becomes much smaller as compared with that of Me_8Fc.

According to Scheme 3, the kinetic equation for the catalytic two-electron reduction of O_2 by Me_8Fc with [(tpfc)Cr^V(O)] is given by eq 8, where the k_{cat} value was determined to be (1.4 ± 0.1) $\times 10^2$ M^{-1} s^{-1} from the slopes of the linear plot of k_{obs} vs [(tpfc)Cr^V(O)] and [O_2] in Figure 10. The turnover frequency in O_2-saturated MeCN was determined from the k_{cat} value (1.4 ± 0.1) $\times 10^2$ M^{-1} s^{-1} and the O_2 concentration (1.3×10^{-2} M) to be 1.8 s^{-1} (eq 8), which is certainly fast enough to observe the electrocatalytic O_2 reduction in Figure 6b. The catalytic cycle with the rate-determining electron transfer form [(tpfc)-Cr^{III}(OH_2)] to O_2 in Scheme 3 was further confirmed by following the time profiles of [(tpfc)Cr^{III}(OH_2)] under stoichiometric conditions. Different amounts of Me_8Fc ($2.0 \times 10^{-5} \sim 1.0 \times 10^{-4}$ M) were injected into a solution of [(tpfc)Cr^V(O)] (1.0×10^{-5} M) containing O_2 (2.6×10^{-3} M), and TFA (1.0×10^{-2} M), [(tpfc)Cr^{III}(OH_2)] was produced rapidly, as shown in Figure 11, where the absorption band at 648 nm due to [(tpfc)Cr^{III}(OH_2)] appeared upon injection. The produced [(tpfc)Cr^{III}(OH_2)] persists for a period of time

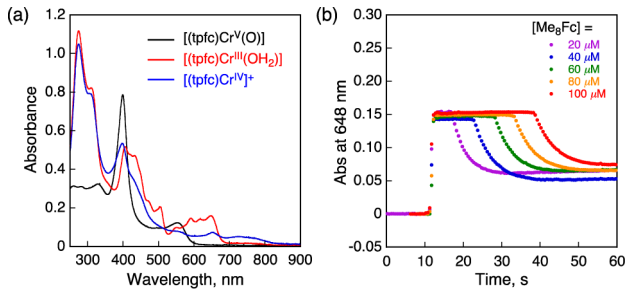

Figure 11. (a) UV−vis spectral changes in the reaction of [(tpfc)Cr^{III}(OH_2)] (1.0×10^{-5} M) with O_2 (2.6×10^{-3} M), Me_8Fc (4.0×10^{-5} M), and TFA (1.0×10^{-2} M). (b) Changes in absorbance at 648 nm (Q-band of [(tpfc)Cr^{III}(OH_2)]) by the addition of various amounts of Me_8Fc $2.0 \times 10^{-5} \sim 1.0 \times 10^{-4}$ M to the solution generated in (a).

dx.doi.org/10.1021/ic5013457 | Inorg. Chem. 2014, 53, 7780−7788

that is proportional to the amount of Me_8Fc added; that is the number of turnovers. Every single turnover takes 5.5 s, based on the average times $(tpfc)Cr^{III}(OH_2)$ persists in each reaction in Figure 11, which leads to a second-order rate constant of $1.4 \times 10^2\ M^{-1}\ s^{-1}$. This value is in excellent agreement with the k_{cat} value determined from the dependence of k_{obs} on the concentrations of $[(tpfc)Cr^{V}(O)]$, TFA, Me_8Fc, and O_2, as shown in Figure 10 (vide supra).

$$d[Me_8Fc^+]/dt = k_{cat}[(tpfc)Cr^{V}(O)][O_2] \quad (8)$$

In order to validate the formation of $[(tpfc)Cr^{III}(OH_2)]$ under steady-state catalysis, EPR measurements were performed, as shown Figure 12. The EPR spectrum obtained

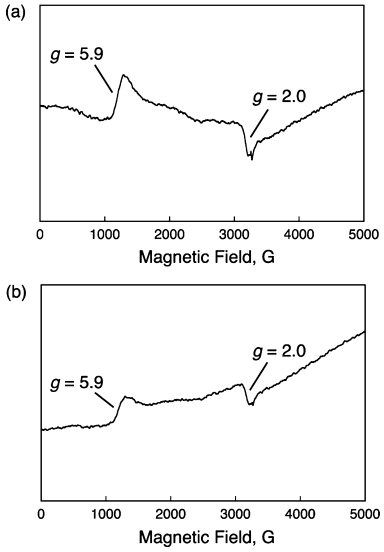

Figure 12. (a) EPR spectrum of $[(tpfc)Cr^{III}(OH_2)]$, generated in situ by mixing $[(tpfc)Cr^{V}(O)]$ (2.5×10^{-4} M) with Me_8Fc (1.0×10^{-3} M) in the presence of TFA (1.0×10^{-3} M) in N_2 saturated MeCN at 77 K. (b) EPR spectrum generated under catalytic conditions at 77 K, where a reaction solution was frozen after the addition of $[(tpfc)Cr^{V}(O)]$ (2.5×10^{-4} M) to a solution containing Me_8Fc (5.0×10^{-3} M), TFA (1.0×10^{-2} M) and O_2 (2.6×10^{-3} M) in air-saturated MeCN. Experimental parameters: microwave frequency, 9.0 GHz; microwave power, 1.0 mW; modulation frequency, 100 kHz; and modulation width, 10 G.

under steady-state catalysis agrees with that of $[(tpfc)Cr^{III}(OH_2)]$ prepared independently, which exhibits a characteristic signal due to $[(tpfc)Cr^{III}(OH_2)]$ ($S = 3/2$) with a zero-field splitting, as reported previously.[40]

Electron Transfer from $[(tpfc)Cr^{III}(OH_2)]$ to O_2. The rate-determining step in the catalytic cycle in Scheme 3 (i.e., the oxidation of $[(tpfc)Cr^{III}(OH_2)]$ by O_2) was examined independently under single-turnover conditions. First, $[(tpfc)Cr^{III}(OH_2)]$ was prepared by adding 2 equiv of Me_8Fc (2.0×10^{-5} M) to the solution of $[(tpfc)Cr^{V}(O)]$ (1.0×10^{-5} M) in the presence of a small or large amount of TFA in deaerated MeCN. Then, O_2 was introduced by mixing an O_2-saturated MeCN solution with a deaerated MeCN solution of $[(tpfc)Cr^{III}(OH_2)]$ using stopped-flow technique. The addition of O_2 to the solution of $[(tpfc)Cr^{III}(OH_2)]$ containing a large excess amount of TFA resulted in the formation of $[(tpfc)Cr^{IV}]^+$, as shown in Figure 13a. In contrast, the addition of O_2 to the solution of $[(tpfc)Cr^{III}(OH_2)]$ containing no acid or a small amount of TFA afforded $[(tpfc)Cr^{V}(O)]$, as shown in Figure 13b.

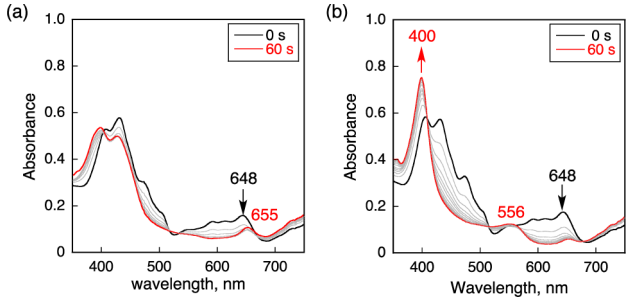

Figure 13. Absorption spectral changes in the oxidation of $[(tpfc)Cr^{III}(OH_2)]$ (1.0×10^{-5} M) by O_2 (6.5×10^{-3} M) in the presence of (a) TFA (1.0×10^{-2} M) in MeCN at 298 K. The black and red lines show the spectra before and after the addition of O_2, respectively. (b) TFA (5.0×10^{-5} M) in MeCN at 298 K. The black and red lines show the spectra before and after the addition of O_2, respectively.

The mechanism of formation for $[(tpfc)Cr^{V}(O)]$ is proposed in Scheme 3, where the dinuclear Cr(IV)-μ-peroxo species $[(tpfc)Cr^{IV}(O_2^{2-})Cr^{IV}(tpfc)]$ is produced via the reduction of $[(tpfc)Cr^{IV}(O_2^{\bullet-})]$ by $[(tpfc)Cr^{III}(OH_2)]$ instead of the reduction of $[(tpfc)Cr^{IV}(O_2^{\bullet-})]$ by Me_8Fc in the presence of large concentrations of TFA to produce the hydroperoxide complex $[(tpfc)Cr^{IV}(OOH)]$ under the catalytic conditions. $[(tpfc)Cr^{IV}(O_2^{2-})Cr^{IV}(tpfc)]$ is consequently converted to $[(tpfc)Cr^{V}(O)]$ via homolytic O−O bond cleavage, as reported previously.[41,42]

The results obtained in this study have significant implications from the perspective of thermodynamics in catalytic O_2 reduction. The formation of $[(tpfc)Cr^{IV}(O_2)$-$Cr^{IV}(tpfc)]$ leading to the production of H_2O is more feasible in the presence of a small amount of proton source. In contrast, under catalytic conditions with a large excess of acid, the formation of the hydroperoxide complex $[(tpfc)Cr^{IV}(OOH)]$ leading to the production of H_2O_2 is more feasible and kinetically favorable. This is the reason $(tpfc)Cr^{V}(O)$, which is a tetragonal complex and left of "oxo wall", acts as a catalyst precursor for selective two-electron reduction of O_2 to produce H_2O_2 rather than the four-electron reduction of O_2 to produce H_2O in the presence of an excess amount of proton source.

■ CONCLUSION

The efficient catalytic two-electron reduction of O_2 by Me_8Fc occurs with a catalytic amount of $[(tpfc)Cr^{V}(O)]$ in the presence of excess TFA in MeCN. The rate-determining step in the catalytic cycle is inner-sphere electron transfer from $[(tpfc)Cr^{III}(OH_2)]$ to O_2 to produce a putative superoxide species $[(tpfc)Cr^{IV}(O_2^{\bullet-})]$. Protonation of the superoxide species is followed by rapid electron transfer (ET) from Me_8Fc to afford the hydroperoxide, which liberates H_2O_2 upon protonation and produces $[(tpfc)Cr^{IV}]^+$. $[(tpfc)Cr^{IV}]^+$ is rapidly reduced back to $[(tpfc)Cr^{III}]$ by electron transfer from Me_8Fc. Interestingly, in the presence of a small amount of TFA, $[(tpfc)Cr^{IV}(O_2^{\bullet-})]$ reacts with $[(tpfc)Cr^{III}(OH_2)]$ to produce the μ-peroxo complex $[(tpfc)Cr^{IV}(O_2^{2-})Cr^{IV}(tpfc)]$, leading to the production of H_2O and $[(tpfc)Cr^{V}(O)]$. In contrast, in the presence of an excess amount of TFA under the catalytic conditions, fast proton-coupled electron transfer (PCET)

dx.doi.org/10.1021/ic5013457 | Inorg. Chem. 2014, 53, 7780−7788

reduction of $[(tpfc)Cr^{IV}(O_2^{\bullet-})]$ by Me_8Fc occurs to produce the hydroperoxide complex $[(tpfc)Cr^{IV}(OOH)]$, leading to the production of H_2O_2 and $[(tpfc)Cr^{IV}]^+$. This is the reason two-electron reduction of O_2 is preferred over four-electron reduction of O_2, even with a Cr complex, despite Cr being to the left of the "oxo wall". This study has paved the way to develop efficient and selective catalysts composed of more earth abundant metals for two-electron reduction of O_2 to H_2O_2.

■ ASSOCIATED CONTENT

Ⓢ Supporting Information

Spectroscopic and kinetic data. This material is available free of charge via the Internet at http://pubs.acs.org.

■ AUTHOR INFORMATION

Corresponding Authors

*E-mail: fukuzumi@chem.eng.osaka-u.ac.jp.
*E-mail: mabuomar@purdue.edu.

Author Contributions

‖These authors contributed equally to this work.

Notes

The authors declare no competing financial interest.

■ ACKNOWLEDGMENTS

This work was supported by an Advanced Low Carbon Technology Research and Development (ALCA) program from Japan Science Technology Agency (JST) to S.F., the Japan Society for the Promotion of Science (JSPS: Grant 20108010 to S.F. and Grant 25·727 to K.M.), and the NSF (Grant CHE-1110475 to M.M.A.-O.).

■ REFERENCES

(1) (a) Pereira, M. M.; Santana, M.; Teixeira, M. *Biochim. Biophys. Acta* **2001**, *1505*, 185. (b) Winter, M.; Brodd, R. J. *Chem. Rev.* **2004**, *104*, 4245. (c) Ferguson-Miller, S.; Babcock, G. T. *Chem. Rev.* **1996**, *96*, 2889.

(2) (a) Hosler, J. P.; Ferguson-Miller, S.; Mills, D. A. *Annu. Rev. Biochem.* **2006**, *75*, 165. (b) Kaila, V. R. I.; Verkhovsky, M. I.; Wikström, M. *Chem. Rev.* **2010**, *110*, 7062.

(3) (a) Von Ballmoos, C.; Lachmann, P.; Gennis, R. B.; Ädelroth, P.; Brzezinski, P. *Biochemistry* **2012**, *51*, 4507. (b) Belevich, I.; Verkhovsky, M. I. *Antioxid. Redox Signaling* **2008**, *10*, 1.

(4) (a) Solomon, E. I.; Ginsbach, J. W.; Heppner, D. E.; Kieber-Emmons, M. T.; Kjaergaard, C. H.; Smeets, P. J.; Tian, L.; Woertink, J. S. *Faraday Discuss.* **2011**, *148*, 11. (b) Solomon, E. I.; Sundaram, U. M.; Machonkin, T. E. *Chem. Rev.* **1996**, *96*, 2563. (c) Farver, O.; Pecht, I. In *Multi-Copper Oxidases*; Messerschmidt, A., Ed.; World Scientific: Singapore, 1997.

(5) (a) Djoko, K. Y.; Chong, L. X.; Wedd, A. G.; Xiao, Z. *J. Am. Chem. Soc.* **2010**, *132*, 2005. (b) Kosman, D. J. *J. Biol. Inorg. Chem.* **2010**, *15*, 15. (c) Farver, O.; Tepper, A. W. J. W.; Wherland, S.; Canters, G. W.; Pecht, I. *J. Am. Chem. Soc.* **2009**, *131*, 18226.

(6) (a) Farver, O.; Pecht, I. In *Multi-Copper Oxidases*; Messerschmidt, A., Ed.; World Scientific: Singapore, 1997. (b) Riva, S. *Trends Biotechnol.* **2006**, *24*, 219. (c) Ward, A. L.; Elbaz, L.; Kerr, J. B.; Arnold, J. *Inorg. Chem.* **2012**, *51*, 4694.

(7) (a) Vielstich, W., Lamm, A., Gasteiger, H. A., Eds.; *Handbook of Fuel Cells: Fundamentals, Technology, and Applications*; Wiley: Chichester, U.K., 2003. (b) Zagal, J. H.; Griveau, S.; Silva, J. F.; Nyokong, T.; Bedioui, F. *Coord. Chem. Rev.* **2010**, *254*, 2755. (c) Li, Z. P.; Liu, B. H. *J. Appl. Electrochem.* **2010**, *40*, 475. (d) Zagal, J. H.; Gulppi, M.; Isaacs, M.; Cárdenas-Jirón, G.; Aguirre, M. J. *Electrochim. Acta* **1998**, *44*, 1349.

(8) (a) Li, W.; Yu, A.; Higgins, D. C.; Llanos, B. G.; Chen, Z. *J. Am. Chem. Soc.* **2010**, *132*, 17056. (b) Gewirth, A. A.; Thorum, M. S. *Inorg. Chem.* **2010**, *49*, 3557. (c) Stambouli, A. B.; Traversa, E. *Renewable Sustainable Energy Rev.* **2002**, *6*, 295. (d) Marković, N. M.; Schmidt, T. J.; Stamenković, V.; Ross, P. N. *Fuel Cells* **2001**, *1*, 105. (d) Steele, B. C. H.; Heinzel, A. *Nature* **2001**, *414*, 345.

(9) (a) Yamazaki, S.; Siroma, Z.; Senoh, H.; Ioroi, T.; Fujiwara, N.; Yasuda, K. *J. Power Sources* **2008**, *178*, 20. (b) Disselkamp, R. S. *Energy Fuels* **2008**, *22*, 2771. (c) Disselkamp, R. S. *Int. J. Hydrogen Energy* **2010**, *35*, 1049.

(10) Fukuzumi, S.; Yamada, Y.; Karlin, K. D. *Electrochim. Acta* **2012**, *82*, 493.

(11) (a) Yamada, Y.; Yoneda, M.; Fukuzumi, S. *Inorg. Chem.* **2014**, *53*, 1272. (b) Yamada, Y.; Yoneda, M.; Fukuzumi, S. *Chem.—Eur. J.* **2013**, *19*, 11733. (c) Yamada, Y.; Yoshida, S.; Honda, T.; Fukuzumi, S. *Energy Environ. Sci.* **2011**, *4*, 2822. (d) Yamada, Y.; Fukunishi, Y.; Yamazaki, S.; Fukuzumi, S. *Chem. Commun.* **2010**, *46*, 7334.

(12) (a) Zhang, J.; Anson, F. C. *J. Electroanal. Chem.* **1993**, *348*, 81. (b) Lei, Y.; Anson, F. C. *Inorg. Chem.* **1994**, *33*, 5003. (c) Weng, Y. C.; Fan, F.-R. F.; Bard, A. J. *J. Am. Chem. Soc.* **2005**, *127*, 17576.

(13) (a) Thorum, M. S.; Yadav, J.; Gewirth, A. A. *Angew. Chem., Int. Ed.* **2009**, *48*, 165. (b) McCrory, C. C. L.; Devadoss, A.; Ottenwaelder, X.; Lowe, R. D.; Stack, T. D. P.; Chidsey, C. E. D. *J. Am. Chem. Soc.* **2011**, *133*, 3696. (c) Thorseth, M. A.; Tornow, C. E.; Tse, E. C. M.; Gewirth, A. A. *Coord. Chem. Rev.* **2013**, *257*, 130. (d) Thorseth, M. A.; Letko, C. S.; Rauchfuss, T. B.; Gewirth, A. A. *Inorg. Chem.* **2011**, *50*, 6158.

(14) Fukuzumi, S. *Chem. Lett.* **2008**, *37*, 808.

(15) (a) Jr, R. M.; Dogutan, D. K.; Teets, T. S.; Suntivich, J.; Shao-Horn, Y.; Nocera, D. G. *Chem. Sci.* **2010**, *1*, 411. (b) Dogutan, D. K.; Stoian, S. A.; McGuire, R., Jr.; Schwalbe, M.; Teets, T. S.; Nocera, D. G. *J. Am. Chem. Soc.* **2011**, *133*, 131. (c) Teets, T. S.; Cook, T. R.; McCarthy, B. D.; Nocera, D. G. *J. Am. Chem. Soc.* **2011**, *133*, 8114.

(16) (a) Anson, F. C.; Shi, C.; Steiger, B. *Acc. Chem. Res.* **1997**, *30*, 437. (b) Shi, C.; Steiger, B.; Yuasa, M.; Anson, F. C. *Inorg. Chem.* **1997**, *36*, 4294. (c) Shi, C. N.; Anson, F. C. *Inorg. Chem.* **1998**, *37*, 1037. (d) Liu, Z.; Anson, F. C. *Inorg. Chem.* **2000**, *39*, 274.

(17) (a) Schechter, A.; Stanevsky, M.; Mahammed, A.; Gross, Z. *Inorg. Chem.* **2012**, *51*, 22. (b) Masa, J.; Ozoemena, K.; Schuhmann, W.; Zagal, J. H. *J. Porphyrins Phthalocyanines* **2012**, *16*, 761.

(18) (a) Olaya, A. J.; Schaming, D.; Brevet, P.-F.; Nagatani, H.; Zimmermann, T.; Vanicek, J.; Xu, H.-J.; Gros, C. P.; Barbe, J.-M.; Girault, H. H. *J. Am. Chem. Soc.* **2011**, *134*, 498. (b) Peljo, P.; Murtomäki, L.; Kallio, T.; Xu, H.-J.; Meyer, M.; Gros, C. P.; Barbe, J.-M.; Girault, H. H.; Laasonen, K.; Kontturi, K. *J. Am. Chem. Soc.* **2012**, *134*, 5974. (c) Su, B.; Hatay, I.; Trojanek, A.; Samec, Z.; Khoury, T.; Gros, C. P.; Barbe, J.-M.; Daina, A.; Carrupt, P.-A.; Girault, H. H. *J. Am. Chem. Soc.* **2010**, *132*, 2655.

(19) (a) Decréau, R. A.; Collman, J. P.; Hosseini, A. *Chem. Soc. Rev.* **2010**, *39*, 1291. (b) Collman, J. P.; Boulatov, R.; Sunderland, C. J.; Fu, L. *Chem. Rev.* **2004**, *104*, 561.

(20) (a) Rosenthal, J.; Nocera, D. G. *Acc. Chem. Res.* **2007**, *40*, 543. (b) Schwalbe, M.; Dogutan, D. K.; Stoian, S. A.; Teets, T. S.; Nocera, D. G. *Inorg. Chem.* **2011**, *50*, 1368. (c) Chang, C. J.; Chng, L. L.; Nocera, D. G. *J. Am. Chem. Soc.* **2003**, *125*, 1866.

(21) (a) Halime, Z.; Kotani, H.; Li, Y.; Fukuzumi, S.; Karlin, K. D. *Proc. Natl. Acad. Sci. U.S.A.* **2011**, *108*, 13990. (b) Chufan, E. E.; Puiu, S. C.; Karlin, K. D. *Acc. Chem. Res.* **2007**, *40*, 563. (c) Kim, E.; Chufan, E. E.; Kamaraj, K.; Karlin, K. D. *Chem. Rev.* **2004**, *104*, 1077.

(22) (a) Carver, C. T.; Matson, B. D.; Mayer, J. M. *J. Am. Chem. Soc.* **2012**, *134*, 5444. (b) Matson, B. D.; Carver, C. T.; Von Ruden, A.; Yang, J. Y.; Raugei, S.; Mayer, J. M. *Chem. Commun.* **2012**, *48*, 11100. (c) Warren, J. J.; Tronic, T. A.; Mayer, J. M. *Chem. Rev.* **2010**, *110*, 6961.

(23) (a) Kakuda, S.; Peterson, R. L.; Ohkubo, K.; Karlin, K. D.; Fukuzumi, S. *J. Am. Chem. Soc.* **2013**, *135*, 6513. (b) Das, D.; Lee, Y.-M.; Ohkubo, K.; Nam, W.; Karlin, K. D.; Fukuzumi, S. *J. Am. Chem. Soc.* **2013**, *135*, 2825. (c) Das, D.; Lee, Y.-M.; Ohkubo, K.; Nam, W.; Karlin, K. D.; Fukuzumi, S. *J. Am. Chem. Soc.* **2013**, *135*, 4018.

(24) (a) Fukuzumi, S.; Karlin, K. D. *Coord. Chem. Rev.* **2013**, *257*, 187. (b) Tahsini, L.; Kotani, H.; Lee, Y.-M.; Cho, J.; Nam, W.; Karlin,

K. D.; Fukuzumi, S. *Chem.—Eur. J.* **2012**, *18*, 1084. (c) Fukuzumi, S.; Kotani, H.; Lucas, H. R.; Doi, K.; Suenobu, T.; Peterson, R. L.; Karlin, K. D. *J. Am. Chem. Soc.* **2010**, *132*, 6874.
(25) (a) Fukuzumi, S.; Mandal, S.; Mase, K.; Ohkubo, K.; Park, H.; Benet-Buchholz, J.; Nam, W.; Llobet, A. *J. Am. Chem. Soc.* **2012**, *134*, 9906. (b) Wada, T.; Maki, H.; Imamoto, T.; Yuki, H.; Miyazato, Y. *Chem. Commun.* **2013**, *49*, 4394.
(26) (a) Kadish, K. M.; Fremond, L.; Shen, J.; Chen, P.; Ohkubo, K.; Fukuzumi, S.; El Ojaimi, M.; Gros, C. P.; Barbe, J. M.; Gullard, R. *Inorg. Chem.* **2009**, *48*, 2571. (b) Chen, P.; Lau, H.; Habermeyer, B.; Gros, C. P.; Barbe, J. M.; Kadish, K. M. *J. Porphyrins Phthalocyanines* **2011**, *15*, 467. (c) Kadish, K. M.; Fremond, L.; Ou, Z.; Shao, J.; Shi, C.; Anson, F. C.; Burdet, F.; Gros, C. P.; Barbe, J.-M.; Guilard, R. *J. Am. Chem. Soc.* **2005**, *127*, 5625.
(27) (a) Chang, C. J.; Deng, Y.; Nocera, D. G.; Shi, C.; Anson, F. C.; Chang, C. K. *Chem. Commun.* **2000**, 1355. (b) Chang, C. J.; Loh, Z. H.; Shi, C.; Anson, F. C.; Nocera, D. G. *J. Am. Chem. Soc.* **2004**, *126*, 10013.
(28) (a) Askarizadeh, E.; Yaghoob, S. B.; Boghaei, D. M.; Slawin, A. M.; Love, J. B. *Chem. Commun.* **2010**, *46*, 710. (b) Volpe, M.; Hartnett, H.; Leeland, J. W.; Wills, K.; Ogunshun, M.; Duncombe, B. J.; Wilson, C.; Blake, A. J.; McMaster, J.; Love, J. B. *Inorg. Chem.* **2009**, *48*, 5195.
(29) (a) Fukuzumi, S.; Mochizuki, S.; Tanaka, T. *Inorg. Chem.* **1989**, *28*, 2459. (b) Fukuzumi, S.; Mochizuki, S.; Tanaka, T. *Inorg. Chem.* **1990**, *29*, 653. (c) Fukuzumi, S.; Mochizuki, S.; Tanaka, T. *J. Chem. Soc., Chem. Commun.* **1989**, 391.
(30) (a) Mase, K.; Ohkubo, K.; Fukuzumi, S. *J. Am. Chem. Soc.* **2013**, *135*, 2800. (b) Honda, T.; Kojima, T.; Fukuzumi, S. *J. Am. Chem. Soc.* **2012**, *134*, 4196. (c) Fukuzumi, S.; Okamoto, K.; Gros, C. P.; Guilard, R. *J. Am. Chem. Soc.* **2004**, *126*, 10441. (d) Fukuzumi, S.; Okamoto, K.; Tokuda, Y.; Gros, C. P.; Guilard, R. *J. Am. Chem. Soc.* **2004**, *126*, 17059.
(31) Fukuzumi, S.; Tahsini, L.; Lee, Y.-M.; Ohkubo, K.; Nam, W.; Karlin, K. D. *J. Am. Chem. Soc.* **2012**, *134*, 7025.
(32) O'Halloran, K. P.; Zhao, C. C.; Ando, N. S.; Schultz, A. J.; Koetzle, T. F.; Piccoli, P. M. B.; Hedman, B.; Hodgson, K. O.; Bobyr, E.; Kirk, M. L.; Knottenbelt, S.; Depperman, E. C.; Stein, B.; Anderson, T. M.; Cao, R.; Geletii, Y. V.; Hardcastle, K. I.; Musaev, D. G.; Neiwert, W. A.; Fang, X. K.; Morokuma, K.; Wu, S. X.; Kogerler, P.; Hill, C. L. *Inorg. Chem.* **2012**, *51*, 7025.
(33) Winkler, J. R.; Gray, H. B. *Struct. Bonding (Berlin, Ger.)* **2011**, *142*, 17−28.
(34) Armarego, W. L. F.; Chai, C. L. L. *Purification of Laboratory Chemicals*, 7th ed; Butterworth−Heinemann : Oxford, 2013.
(35) (a) Edwards, N. Y.; Eikey, R. A.; Loring, M. I.; Abu-Omar, M. M. *Inorg. Chem.* **2005**, *44*, 3700. (b) Eikey, R. A.; Abu-Omar, M. M. *Coord. Chem. Rev.* **2003**, *243*, 83.
(36) (a) Meier-Callahan, A. E.; Gray, H. B.; Gross, Z. *Inorg. Chem.* **2000**, *39*, 3605. (b) Gross, Z.; Golubkov, G.; Simkhovich, L. *Angew. Chem., Int. Ed.* **2000**, *39*, 4045. (c) Golubkov, G.; Bendix, J.; Gray, H. B.; Mahammed, A.; Goldberg, I.; DiBillio, A. J.; Gross, Z. *Angew. Chem., Int. Ed.* **2001**, *40*, 2132.
(37) (a) Fukuzumi, S.; Imahori, H.; Yamada, H.; El-Khouly, M. E.; Fujitsuka, M.; Ito, O.; Guldi, D. M. *J. Am. Chem. Soc.* **2001**, *123*, 2571. (b) Fukuzumi, S.; Ohkubo, K.; Chen, Y.; Pandey, R. K.; Zhan, R.; Shao, J.; Kadish, K. M. *J. Phys. Chem. A* **2002**, *106*, 5105.
(38) Fukuzumi, S.; Kuroda, S.; Tanaka, T. *J. Am. Chem. Soc.* **1985**, *107*, 3020.
(39) Mann, C. K.; Barnes, K. K. In *Electrochemical Reactions in Nonaqueous Systems*; Mercel Dekker: New York, 1970.
(40) Meier-Callahan, A. E.; Di Bilio, A. J.; Simkhovich, L.; Mahammed, A.; Goldberg, I.; Gray, H. B.; Gross, Z. *Inorg. Chem.* **2001**, *40*, 6788.
(41) Mahammed, A.; Gray, H. B.; Meier-Callahan, A. E.; Gross, Z. *J. Am. Chem. Soc.* **2003**, *125*, 1162.
(42) O'Reilly, M. E.; Del Castillo, T. J.; Falkowski, J. M.; Ramachandran, V.; Pati, M.; Correia, M. C.; Abboud, K. A.; Dalal, N. S.; Richardson, D. E.; Veige, A. S. *J. Am. Chem. Soc.* **2011**, *133*, 13661.